ADVANCED MATERIALS

Supporting Information

for *Adv. Mater.*, DOI: 10.1002/adma.201600859

Organolead Halide Perovskites for Low Operating Voltage Multilevel Resistive Switching

Jaeho Choi, Sunghak Park, Joohee Lee, Kootak Hong, Do-Hong Kim, Cheon Woo Moon, Gyeong Do Park, Junmin Suh, Jinyeon Hwang, Soo Young Kim, Hyun Suk Jung, Nam-Gyu Park, Seungwu Han, Ki Tae Nam, and Ho Won Jang**

Supporting Information

Organolead Halide Perovskites for Low Operating Voltage Multilevel Resistive Switching

Jaeho Choi[†] and Sunghak Park[†], Joohee Lee, Kootak Hong, Do-Hong Kim, Cheon Woo Moon, Gyeong Do Park, Junmin Suh, Jinyeon Hwang, Soo Young Kim, Hyun Suk Jung, Nam-Gyu Park, Seungwu Han, Ki Tae Nam*, Ho Won Jang*

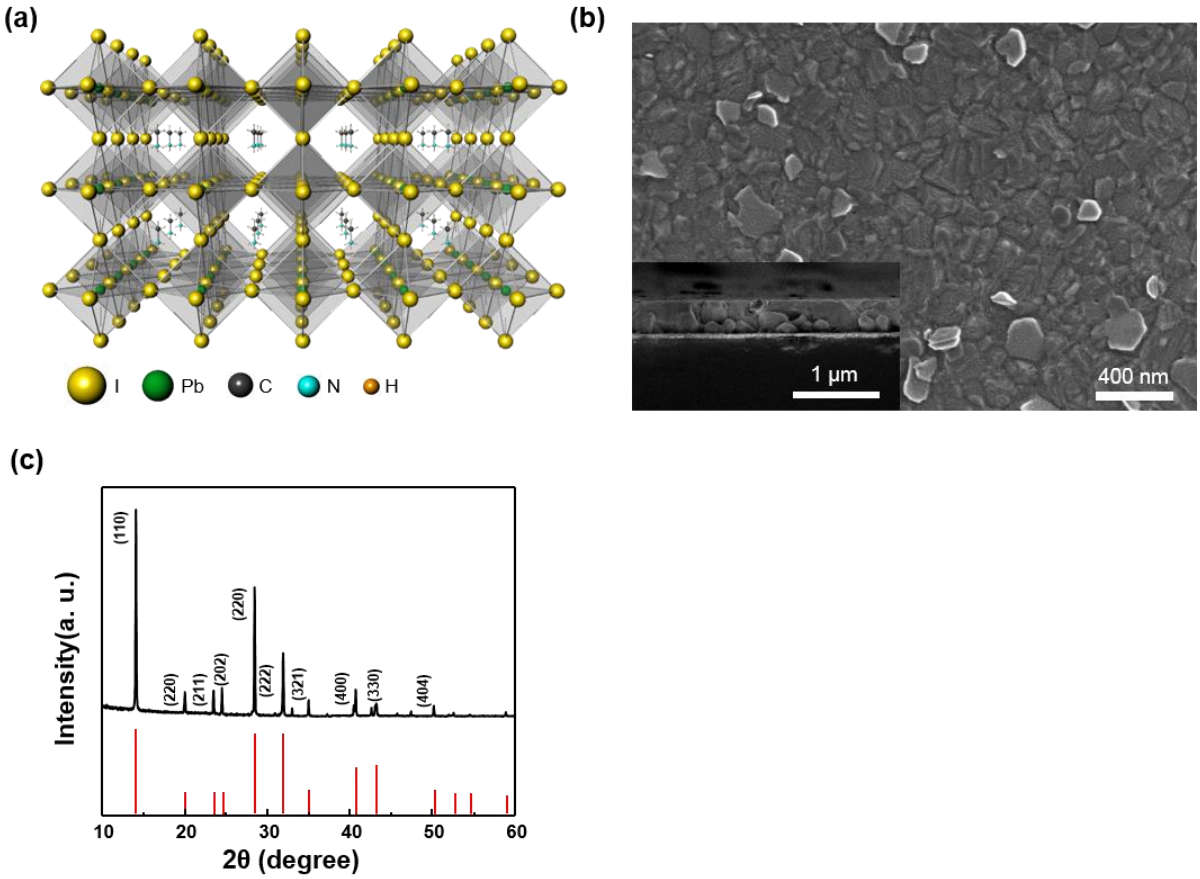

Figure S1. Crystal structure of $CH_3NH_3PbI_3$ and X-ray diffraction pattern. (a) Crystal structure of $CH_3NH_3PbI_3$. (b) Plane-view and cross-sectional SEM images of a 400 nm-thick $CH_3NH_3PbI_3$ thin film on $Pt/Ti/SiO_2/Si$ substrate. (c) X-ray diffraction pattern of a $CH_3NH_3PbI_3$ film on SiO_2/Si substrate. Red lines are XRD pattern from Ref. 17

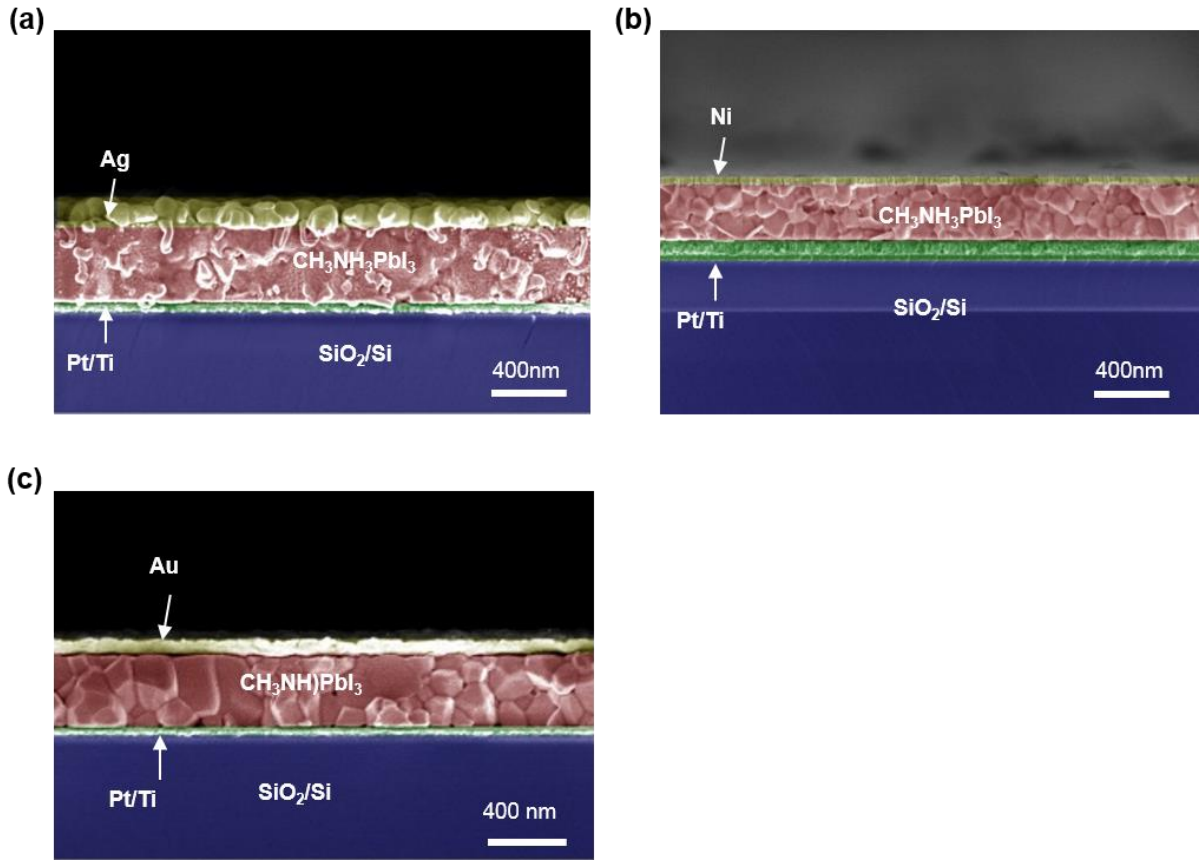

Figure S2. Cross-sectional SEM images of the vertical structure devices. (a)-(c), Each device has (a) Ag, (b) Ni (c) Au electrodes. The thickness of $CH_3NH_3PbI_3$ thin film is about 320-400nm. We adopted two types of metals, such as Ag and Ni to the top electrodes to investigate the resistive switching properties. The minimum thickness of the top electrodes is about 50 nm. In the cross-sectional SEM image of (c), the electro-migration of the Ag top electrodes occurs under the electric field from a field emission cathode in an electron gun during taking the cross-sectional SEM image of the devices. The electro-migrated Ag looks like worm.

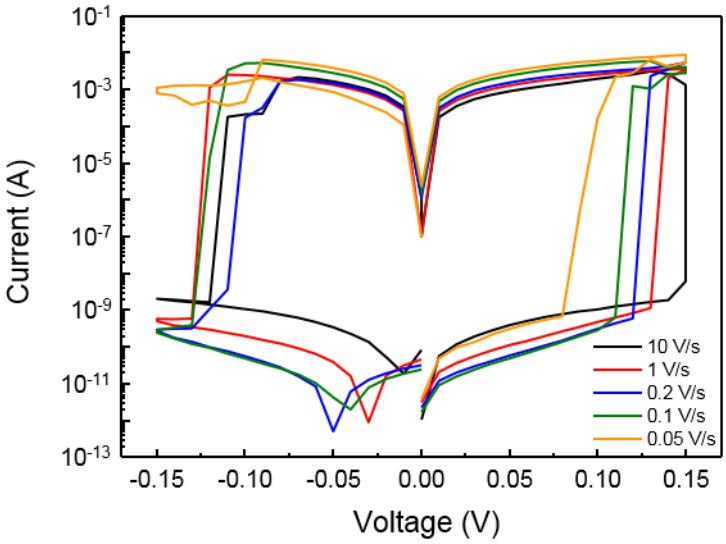

Figure S3. *I-V* characteristics of Ag/$CH_3NH_3PbI_3$/Pt cells with the control of scan rates.

Table S1. The variation of switching voltages by the control of scan rates in the *I-V* measurement.

Scan rate (V/s)	15.625	10	1	0.2	0.1	0.05
Switching voltage (V)	0.15	0.15	0.14	0.13	0.12	0.11

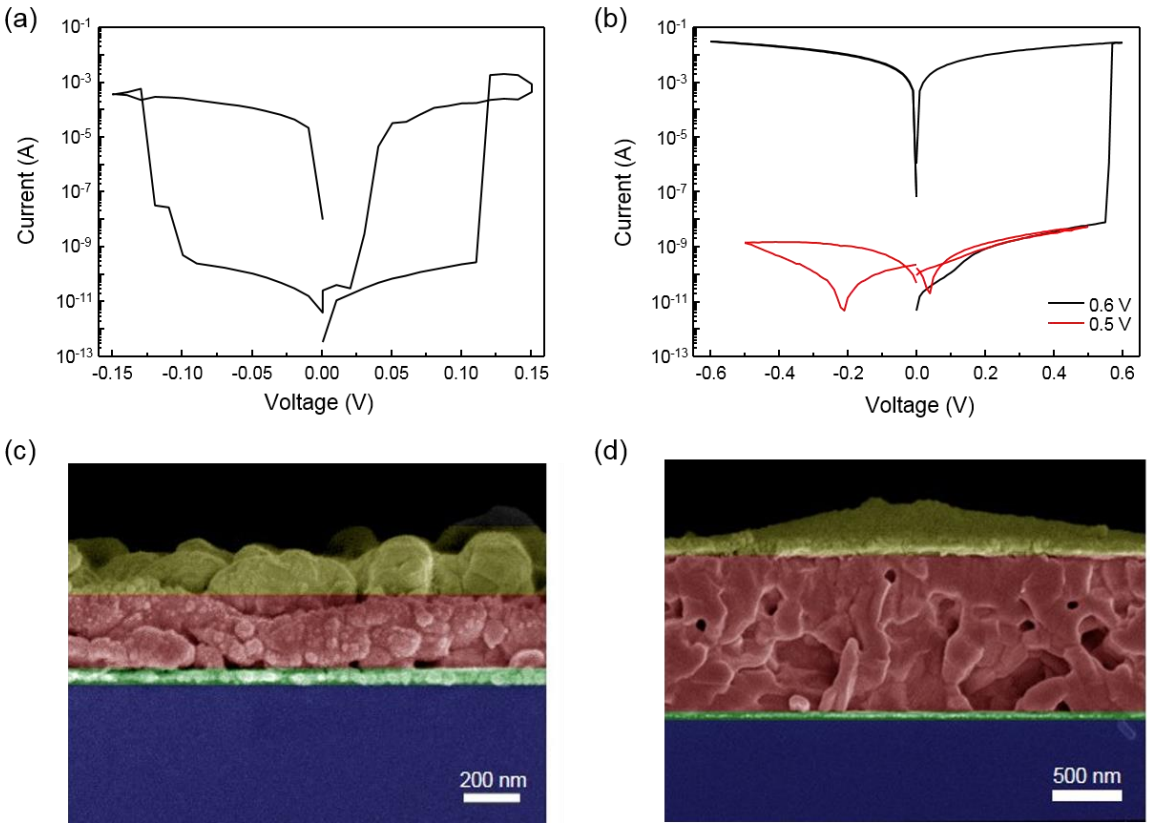

Figure S4. Resistive switching properties of Ag/$CH_3NH_3PbI_3$/Pt devices. *I-V* characteristics of Ag/$CH_3NH_3PbI_3$/Pt cells which adopt (a) 220-nm-thick and (b) 1.1-μm-thick $CH_3NH_3PbI_3$ films. Cross-sectional SEM images of (c) Ag/$CH_3NH_3PbI_3$ (220-nm-thick)/Pt and (d) Ag/$CH_3NH_3PbI_3$ (1.1-μm-thick)/Pt devices.

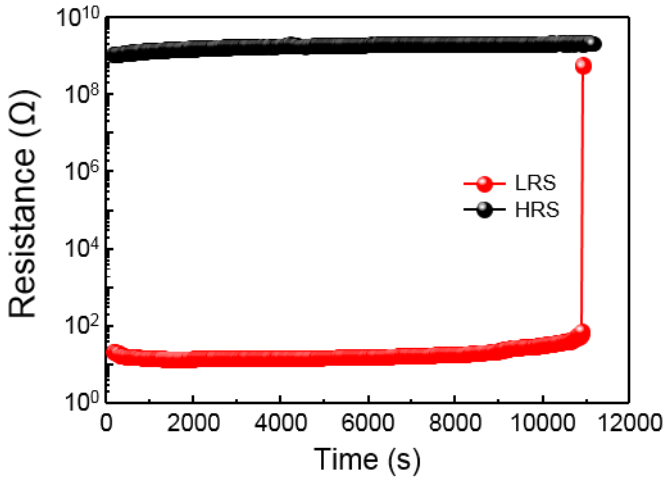

Figure S5. Retention characteristics of the $CH_3NH_3PbI_3$ device.

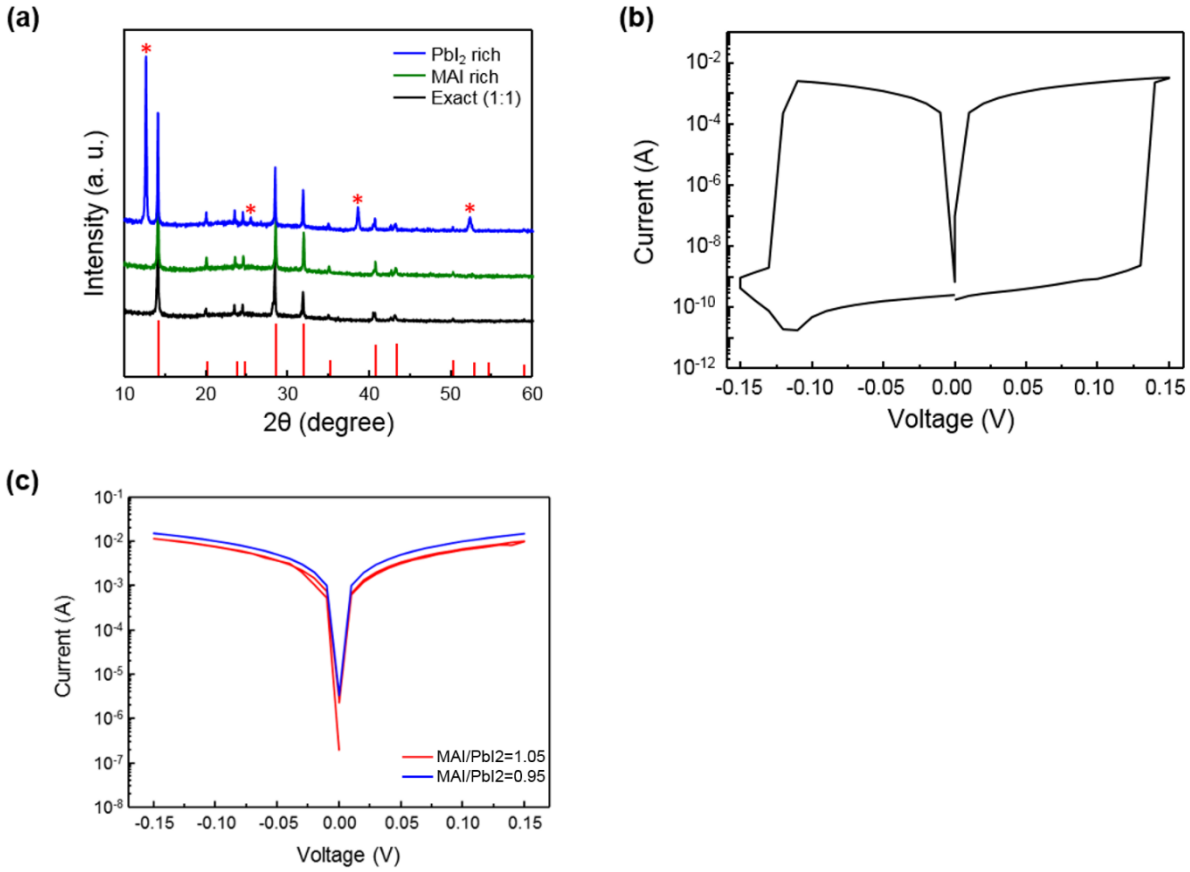

Figure S6. Stoichiometry-dependent *I-V* characteristics of $CH_3NH_3PbI_3$ devices**.** (a) X-ray diffraction patterns of a $CH_3NH_3PbI_3$ films by the controlling of the ratio of methylammonium and lead iodide. (Black line-exact stoichiometry, green line-methylammonium iodide rich, blue line-lead iodide rich, red line-Ref 17.). In the blue line, peaks for PbI_2 appear at 12.67, 25.49, 38.59, and 52.33 degrees (Red stars, JCPDS No. 00-007-0235). *I-V* characteristics of (b) the stoichiometric $CH_3NH_3PbI_3$ film (the ratio of methylammonium iodide (MAI) and lead iodide (PbI_2) precursors = 1:1) and (c) MAI-rich (MAI/PbI_2 = 1.05) and PbI_2-rich (MAI/PbI_2 = 0.95) films.

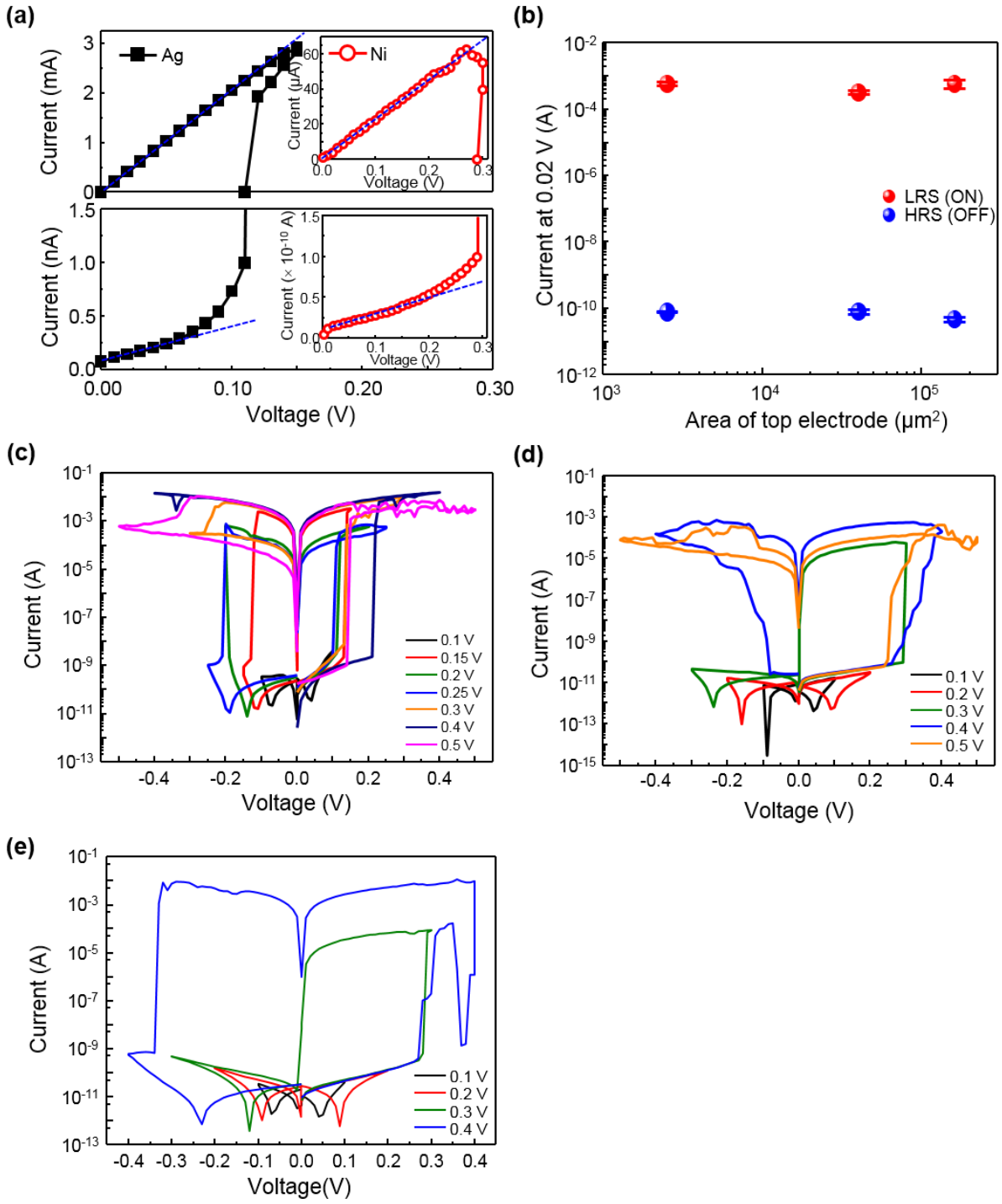

Figure S7. Dependence of the top electrodes and electrode area. (a) Linear-scale *I-V* characteristics of the ON (LRS) and OFF states. (b) Dependence of ON and OFF state current levels on the area of Ag top electrodes for Ag/$CH_3NH_3PbI_3$/Pt cells. (c) Ag/$CH_3NH_3PbI_3$/Pt, (d) Ni/$CH_3NH_3PbI_3$/Pt and (e) Au/$CH_3NH_3PbI_3$/Pt cells. The cells adopt (c) Ag, (d) Ni and (e) Au top electrodes show hysteretic *I-V* curves which are applicable to resistive switching. The cells with Ag top electrodes are switchable in low SET/RESET voltage. With high SET voltage (> 0.25 V), these cells could not be turned off perfectly. The cells adopt Ni and Au top electrodes had relatively higher SET voltages (> 0.3 V).

Table S2. Five $CH_3NH_3PbI_3$ films with different grain sizes by controlling annealing condition.

	Annealing temperature (℃)	Time (min)	Annealing atmosphere	Average grain size (nm)	Standard deviation of grain size (nm)	Endurance (cycles)
Sample 1	100	40	DMF	601.30	±74.17	0
Sample 2	100	40	Ambient	147.06	±22.86	4
Sample 3	70	40	Ambient	103.35	±10.47	50
Sample 4	70	1	Ambient	89.45	±6.75	38
Sample 5	No annealing	N/A	Ambient	71.15	±5.39	17

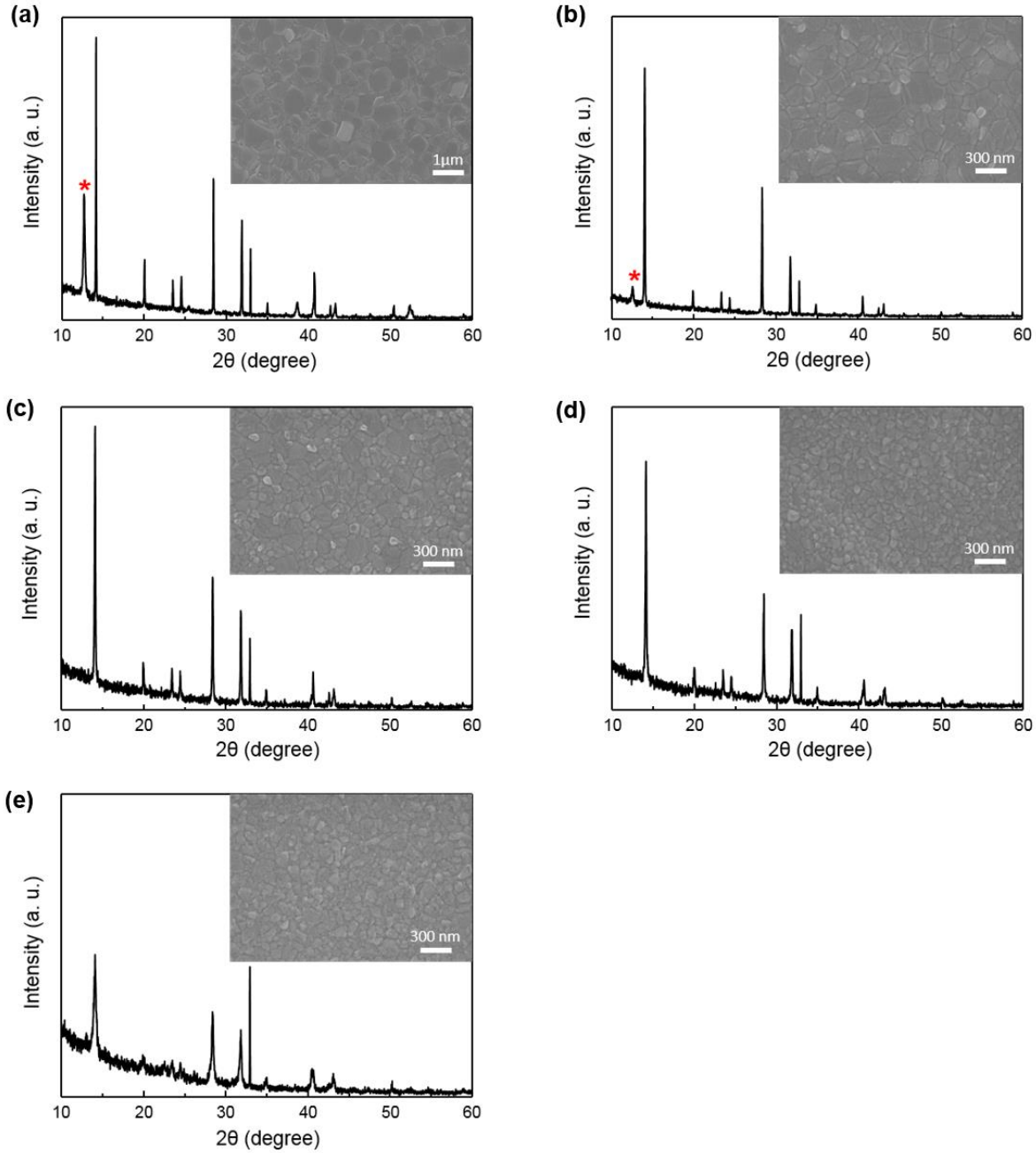

Figure S8. X-ray diffraction patterns and SEM images for $CH_3NH_3PbI_3$ films synthesized using annealing conditions. (a) Sample 1 (100 °C, 40mins, DMF), (b) Sample 2 (100 °C, 40 mins, ambient), (c) Sample 3 (70 °C, 40 mins, ambient), (d) Sample 4 (70 °C, 1 min, ambient), (e) Sample 5 (No heat treatment, ambient). The diffraction peak near 12.6° for PbI_2 (Red star, 6a) is absent. The insets of each XRD pattern are plain-view SEM images of each sample.

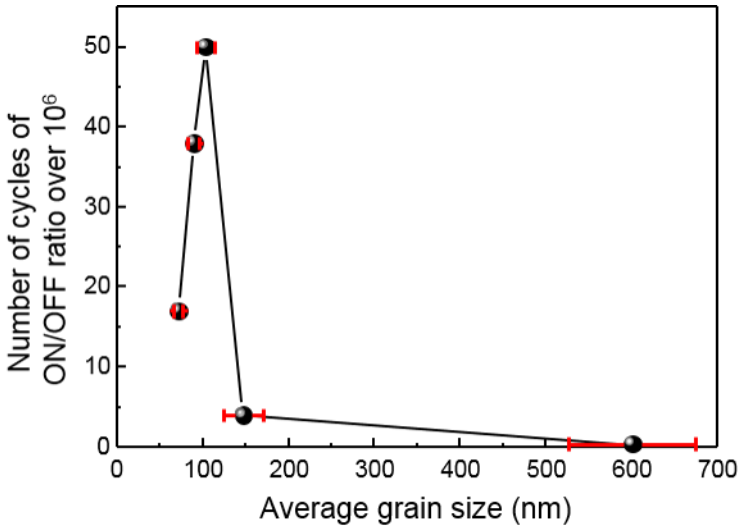

Figure S9. Number of cycles with ON/OFF ratio over 10^6 from endurance measurements (total 50 number of cycles) for $CH_3NH_3PbI_3$ films with different grain sizes.

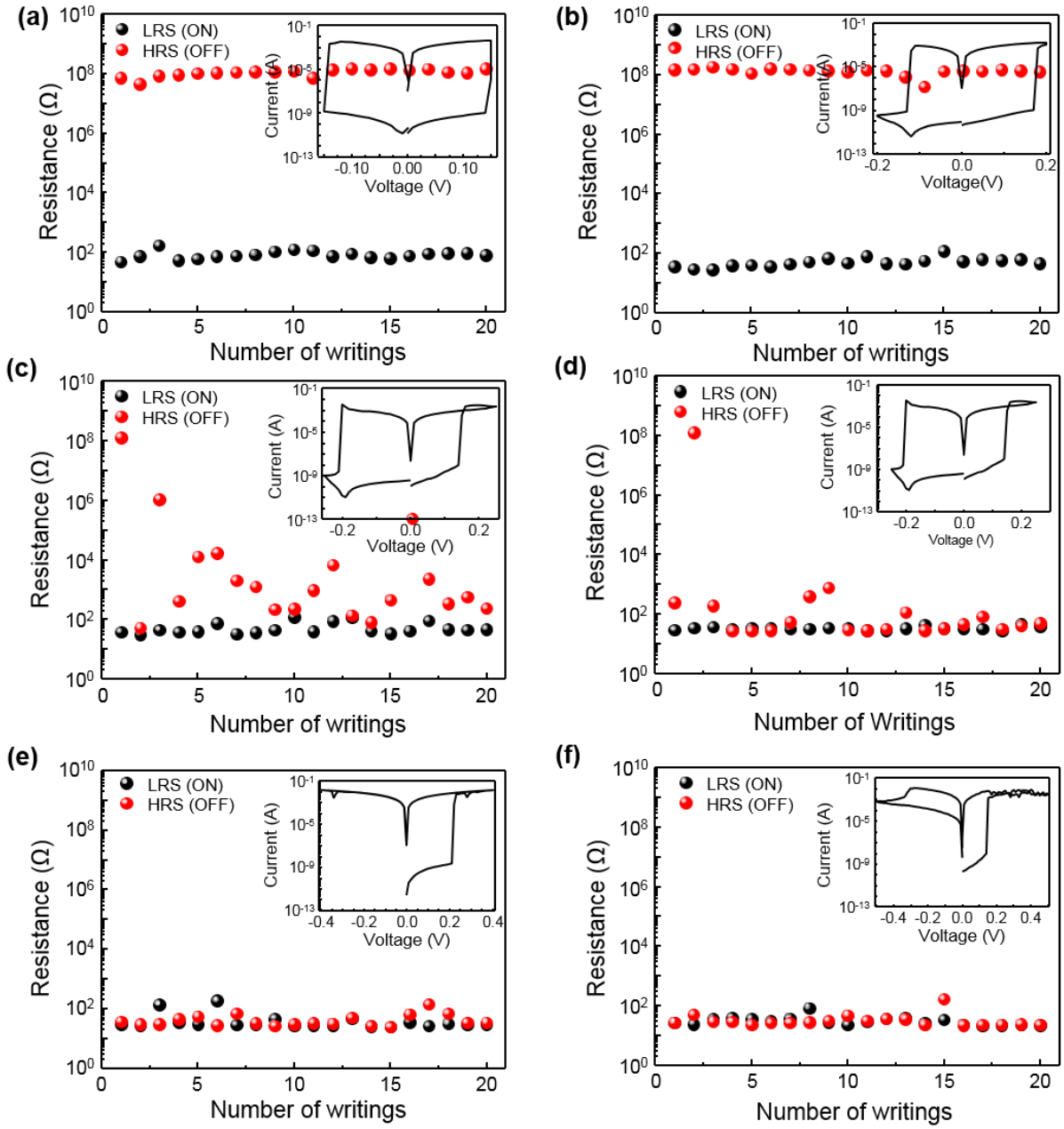

Figure S10. Binary on-off operation of $CH_3NH_3PbI_3$ thin film with Ag top electrode. Switching with various pulse voltages (a) ± 0.15 V, (b) ± 0,2 V, (c) ± 0.25 V, (d) ± 0.3 V, (e) ± 0.4 V, and (f) ±0.5V. The pulse width is fixed to 250 ms. When the voltage of the pulse is over 0.25 V, reversible switching becomes impossible. The insets of each figure show voltage sweeps for the virgin cells. The voltage sweeps are performed 0 V → (+) V → 0 V → (-) V → 0 V.

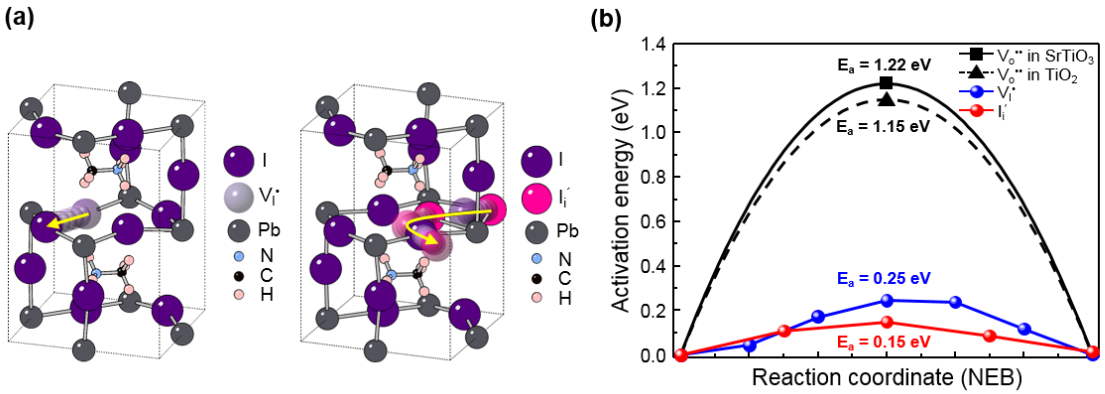

Figure S11. DFT calculation about the migration of iodine vacancies and iodine interstitials in $CH_3NH_3PbI_3$. (a) The schematic of migration paths for iodine vacancies, $V_I^{\bullet}$, and interstitials, I_i' in the unit cell of $CH_3NH_3PbI_3$. (b) DFT calculation about the activation energy for the movements of $V_I^{\bullet}$ and I_i' to the next sites. The potential energy as the $V_I^{\bullet}$ (black), I_i' (red), $V_o^{\bullet\bullet}$ in $SrTiO_3$ (black, solid), and $V_o^{\bullet\bullet}$ in TiO_2 (black, dash) move to the next sites. $V_I^{\bullet}$ and I_i' in $CH_3NH_3PbI_3$ can migrate with low activation energies of 0.25 eV and 0.15 eV. However, the migration barriers of $V_O^{\bullet\bullet}$ in TiO_2 and $SrTiO_3$ are 1.15 eV and 1.22 eV each.

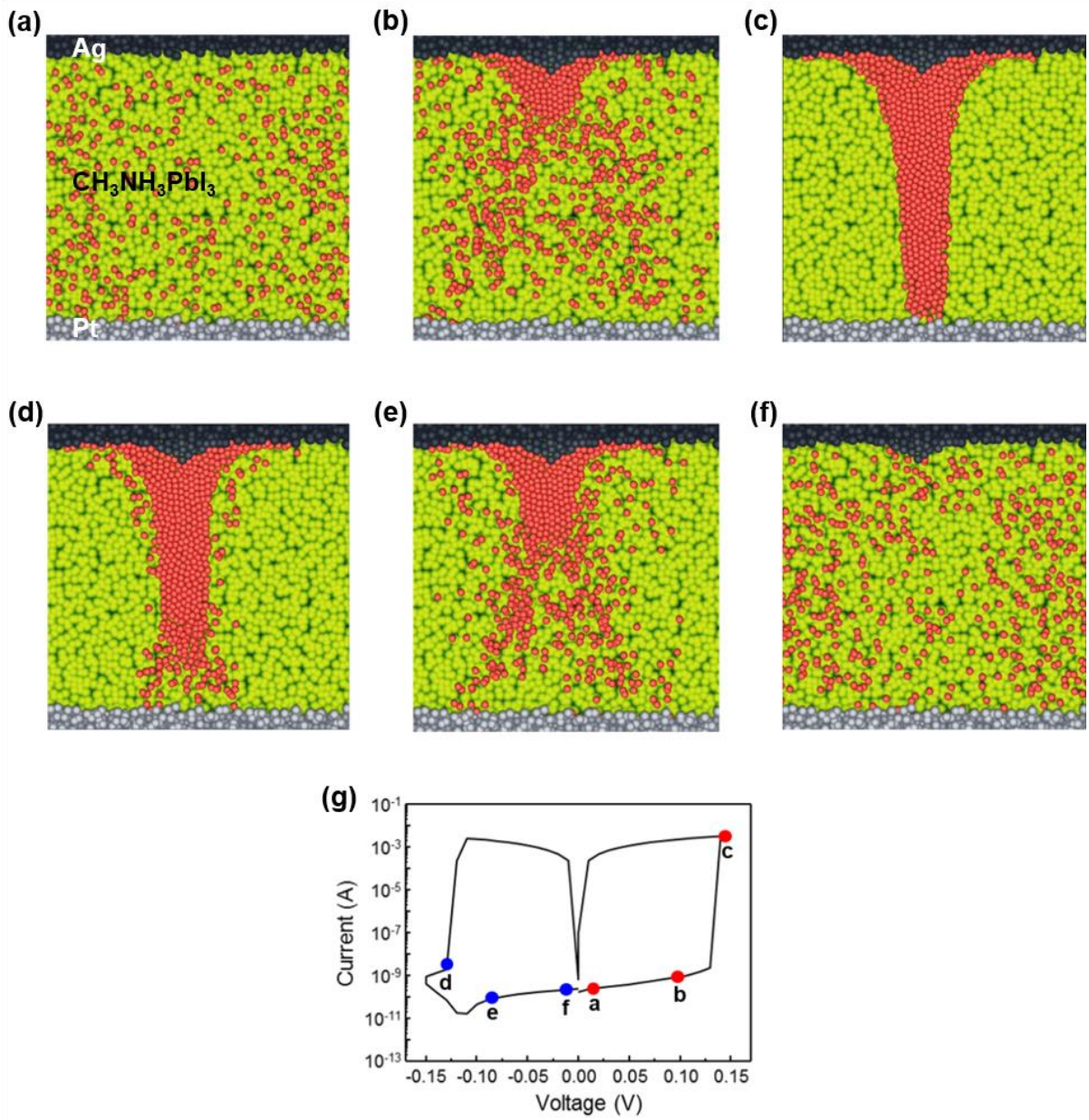

Figure S12. Schematic of filamentary resistive switching behavior in $Ag/CH_3NH_3PbI_3/Pt$ cells by defect ion migration. (a) Initial state of $Ag/CH_3NH_3PbI_3/Pt$ cells with iodine interstitials ($I_i^{'}$). (b) Ion migration of iodine interstitials by applying positive electric field (+ 0.15 V). (c) Fully formed conducting filament (ON state). (d), (e) Ion migration of iodine interstitials by applying negative electric field (- 0.15 V). (f) Rupture of the conducting filament (OFF state). (g) Corresponding *I-V* curve.

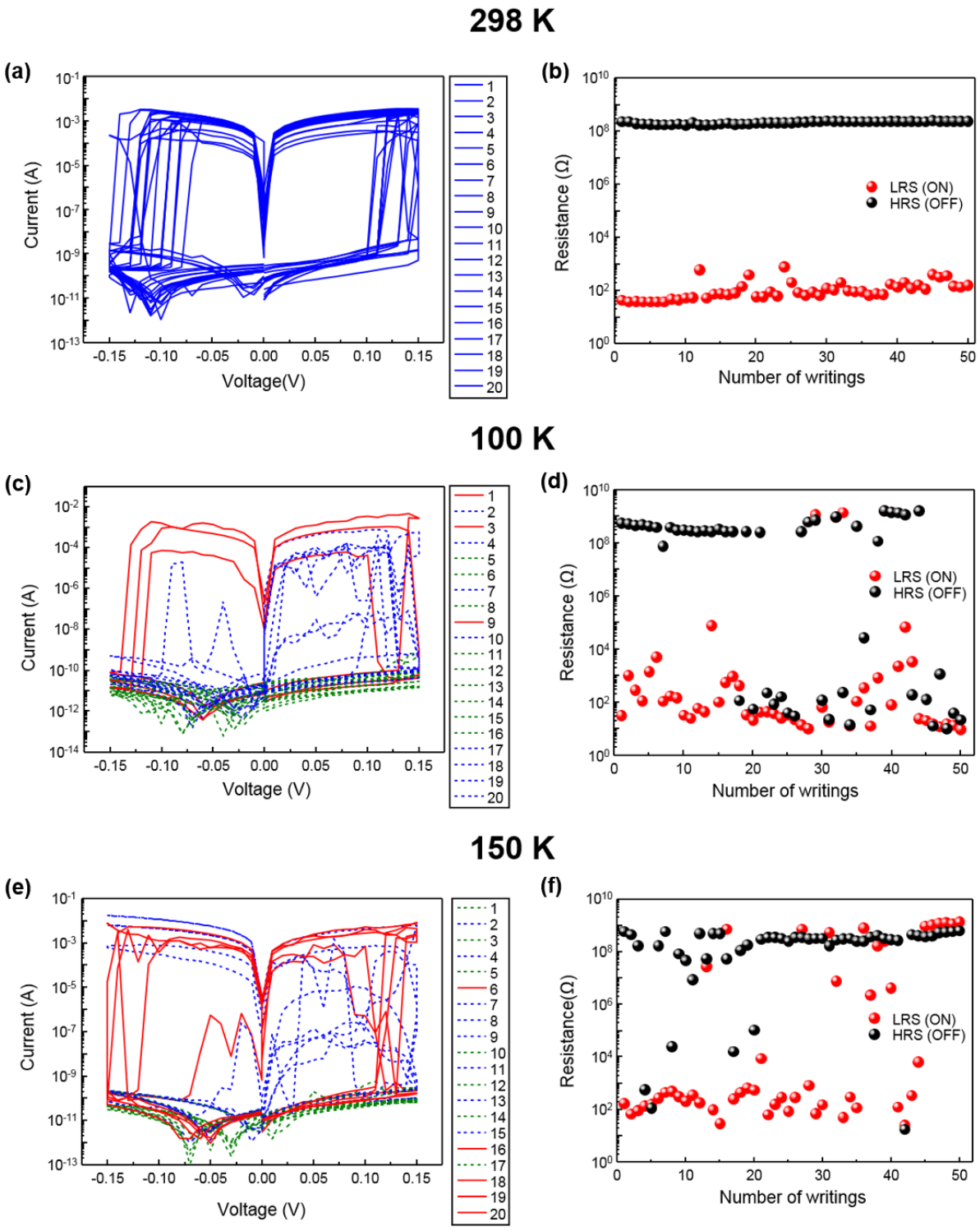

Figure S13. Resistive switching properties of Ag/$CH_3NH_3PbI_3$/Pt cells measured at different temperatures. (a) *I-V* curves of 20 cells measured at room temperature. (b) The endurance of a cell measured at room temperature. (c) *I-V* curves of 20 cells measured at 100 K. (d) The endurance of a cell measured at 100 K. (e) *I-V* curves of 20 cells measured at 150 K. (f) The endurance of a cell measured at 150 K.

The temperature dependent resistive switching behaviour of Ag/$CH_3NH_3PbI_3$/Pt cells can be can be explained by the field-induced ionic drift velocity which is expressed by the formula[54]

$$v \approx fae^{\frac{-U_A^{eff}}{k_B T}}$$

, where f is the frequency of escape attempts, a is the migration distance, and U_A^{eff} is an effective potential barrier $U_A - \frac{qaE}{2}$, which is approximated as U_A in low field like in this study. When we assume the potential barrier for migration of ion, U_A as 0.15 eV, the migration barrier of the split-interstitials in this study, the drift velocity slows down to the 0.3 % of the room-temperature velocity at 150 K, and to the 0.001 % at 100 K. We believe that the result is the strong evidence which the ionic migration is responsible for the resistive switching mechanism in the Ag/$CH_3NH_3PbI_3$/Pt cells.

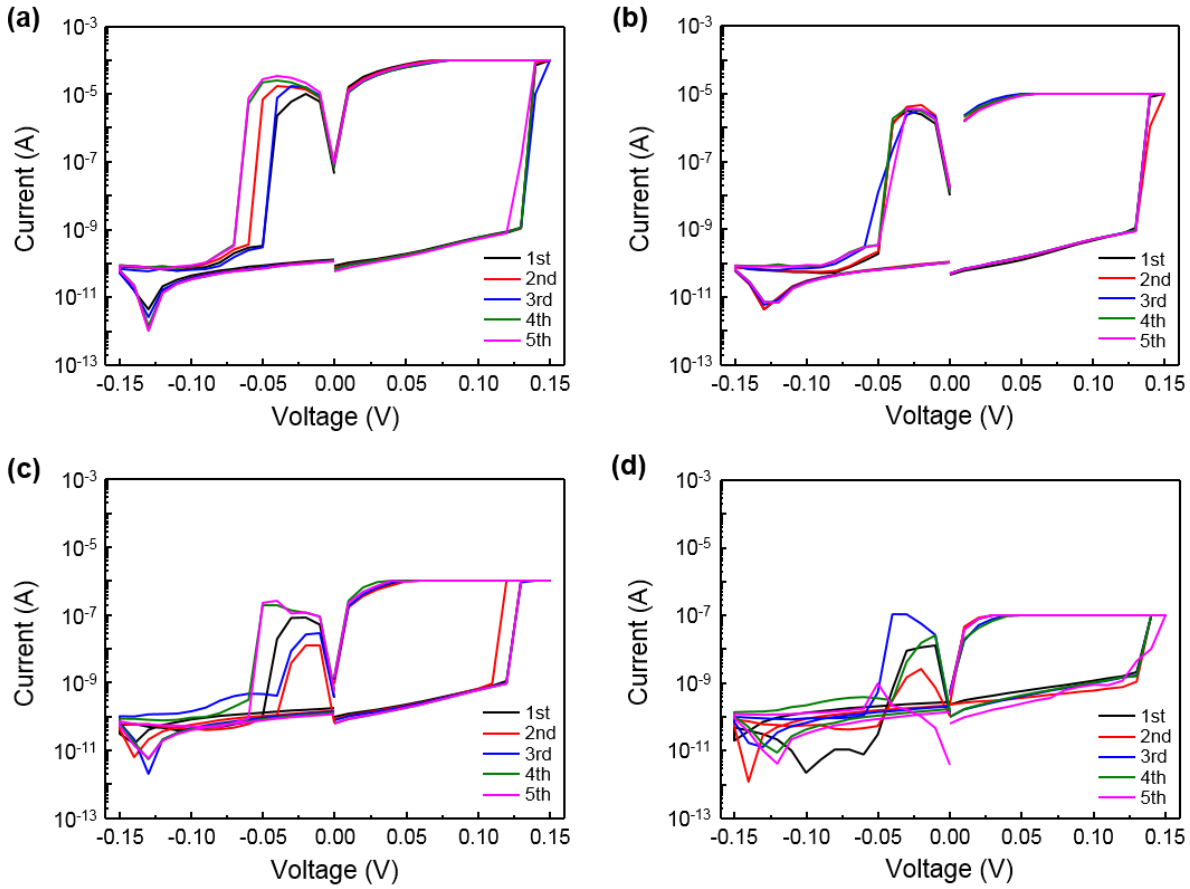

Figure S14. Dependence of the compliance currents in switching pulses. *I-V* characteristics with various current compliances of (a) 10^{-4} A, (b) 10^{-5} A, (c) 10^{-6} A, and (d) 10^{-7} A. The *I-V* curves which measured under the current compliances of 10^{-4} A, 10^{-5} A, and 10^{-6} A show hysteretic characteristics for non-volatile memories. But, the *I-V* curves which measured under 10^{-7} of the current compliance show an unstable and non-switchable result .

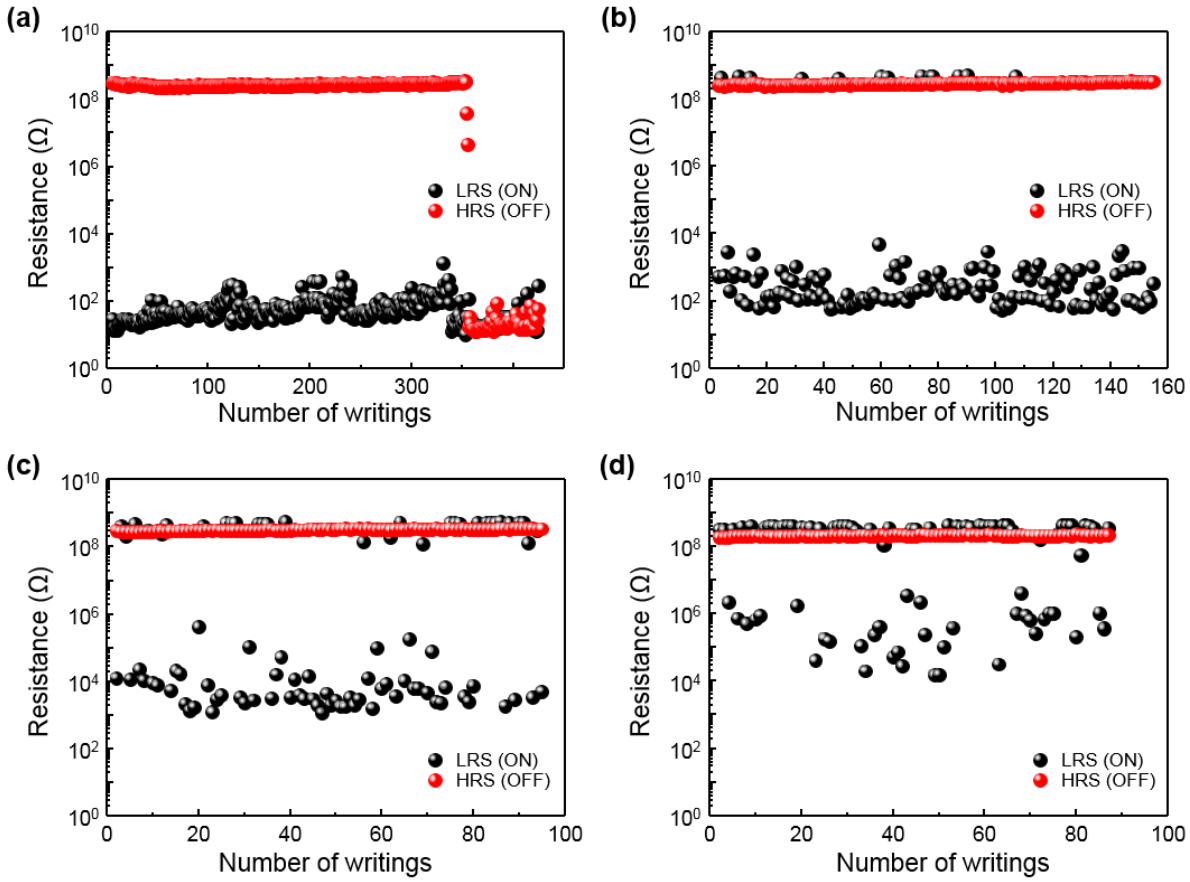

Figure S15. Dependence of the compliance currents in switching pulses. (a)-(d), Switching with various current compliances of (a) 10^{-2} A, (b) 10^{-4} A, (c) 10^{-5} A, and (d) 10^{-6} A. The voltage of the switching pulses is 0.15 V. The pulse width is fixed to 250 ms. As illustrate in the figure, 10^{-2} A of the current compliance for reversible switching shows the most stable result. When the current compliance of the pulse is under 10^{-6} A, the reversible switching is impossible. With decreasing the current compliance of the switching pulses, a percent, the reversible switching is accurate, is decreasing. It is obvious that the higher current compliance for the reversible switching is applied, the better switching accuracy is performed.

Reference

[55] D. B. Strukov, R. S. Williams, *Appl. Phys. A.* **2009**, 94, 515.